BIOMEDICAL ENGINEERING MSc PROGRAM
UNIVERSITY OF CRETE
TECHNICAL UNIVERSITY OF CRETE
FOUNDATION FOR RESEARCH AND TECHNOLOGY-HELLAS

University of Crete

Medical School

Biomedical Engineering MSc Program

"Multifunctional scaffolds for bone tissue engineering: synthesis, characterization and in vitro evaluation"

Anna Papaioannou

Supervising Professors: Maria Vamvakaki, Maria Chatzinikolaidou

Evaluation Committee: Maria Vamvakaki, Maria Chatzinikolaidou, Anna Mitraki

Heraklion 2022

Πανεπιστήμιο Κρήτης

Ιατρική Σχολή

ΔΠΜΣ στη Βιοϊατρική Μηχανική

"Πολυλειτουργικά Τρισδιάστατα Ικριώματα για εφαρμογές στη Μηχανική Ιστού: Σύνθεση, Χαρακτηρισμός και Αξιολόγηση *In Vitro* "

Άννα Παπαϊωάννου

Επιβλέπουσες Καθηγήτριες: Μαρία Βαμβακάκη, Μαρία Χατζηνικολαΐδου

Τριμελής Επιτροπή: Μαρία Βαμβακάκη, Μαρία Χατζηνικολαΐδου, Άννα Μητράκη

Ηράκλειο 2022

Table of Contents

Abstract

Hydrogels have been widely exploited for biomedical applications such as contact lenses, drug delivery. Their special properties of large pore size for permeation of nutrients, high swelling degrees and water absorption, cell encapsulation and also tunable mechanical properties make them the perfect candidates for tissue engineering applications as well. Photopolymerizable hydrogels synthesis can be an advantageous method in tissue engineering, introducing fast reaction rates, in situ gel formation at physiological temperatures and spatiotemporal control of polymerization. The main disadvantage of photopolymerization lies in the use of UV light for photoinitiation and photocrosslinking which can be toxic for the cells and can have adverse effects to their metabolic activity.

This first part of this thesis, aims at the synthesis of photopolymerizable hydrogels by employing g-C_3N_4, widely known as a visible light photocatalyst as a visible light photoinitiator. Nanosheets of the photoinitiator that were synthesized employing two different green exfoliation methods were assessed for their biocompatibility and also three different photopolymerizable derivatives from dopamine, gelatin and alginate were synthesized to be explored in the hydrogel synthesis of copolymeric hydrogels. To establish the optimum reaction conditions, commercially available poly(ethylene glycol methyl ether methacrylate) with a molecular weight of 475 g/mol (PEGMA, M_w = 475 g/mol) was copolymerized with the in-house synthesized dopamine methacrylamide (DMA) comonomer via free-radical polymerization photo-initiated by g-C_3N_4 to obtain PEGMA-*co*-DMA hydrogels The catechol moieties of DMA enabled the self-crosslinking of the polymeric chains via hydrogen bonding, thus eliminating the need for an additional, and often toxic, cross-linker. The as-synthesized hydrogels exhibited swelling profiles which were dependent on their cross-link density, and remarkable degrees of swelling up to 2000%.

Περίληψη

Οι υδρογέλες (hydrogels) έχουν αξιοποιηθεί σε πληθώρα βιοιατρικών εφαρμογών, όπως είναι οι φακοί επαφής και τα συστήματα μεταφοράς φαρμάκων. Λόγω των εξαιρετικών τους ιδιοτήτων, όπως είναι η πορώδης μορφολογία τους που επιτρέπει την διέλευση θρεπτικών ουσιών, η ικανότητά τους να προσροφούν μεγάλες ποσότητες νερού (swelling), η δυνατότητα ελέγχου των μηχανικών τους ιδιοτήτων κατά τη σύνθεση αλλά και η ικανότητα ενθυλάκωσης κυττάρων (cell encapsulation), οι υδρογέλες αποτελούν εξαιρετικά υλικά για την εφαρμογή τους ως τρισδιάστατα ικριώματα για εφαρμογές στη μηχανική ιστού. Η σύνθεση υδρογελών με φώτο-πολυμερισμό φέρει πολλά πλεονεκτήματα για την εφαρμογή τους σε αυτό το πεδίο, όπως είναι η μικρή χρονική διάρκεια αντιδράσεων, η ικανότητα πολυμερισμού in situ σε φυσιολογικές θερμοκρασίες και ο ελεγχόμενος χωρικά και χρονικά πολυμερισμός. Το βασικό μειονέκτημα αυτών των πολυμερισμών βρίσκεται στη χρήση φωτός στην περιοχή του υπεριώδους (UV) για την φώτο-εκκίνηση (photoinitiation) και την φώτο-διασταύρωση (photocrosslinking) , καθώς αυτή η ακτινοβολία μπορεί να είναι τοξική για τα κύτταρα ή/και να προκαλέσει παρενέργειες στις μεταβολικές διεργασίες των κυττάρων.

Στόχος αυτής της εργασίας είναι η σύνθεση φώτο-πολυμεριζόμενων υδρογελών χρησιμοποιώντας το g-C_3N_4, γνωστό στο πεδίο της φώτο-κατάλυσης με ορατό φως, σαν έναν εκκινητή που διεγείρεται με ορατό φως (visible light initiator), Οι νάνο-μορφολογίες του εκκινητή που συντέθηκαν με δύο πράσινες μεθόδους, ελέγχθηκαν ως προς τη βιοσυμβατότητα τους και επίσης ντοπαμίνη, ζελατίνη και αλγινικό οξύ τροποποιήθηκαν με μεθακρυλομάδες για να χρησιμοποιηθούν στη σύνθεση συμπολυμερικών υδρογελών. Για να οριστούν οι βέλτιστες συνθήκες της αντίδρασης, το εμπορικά διαθέσιμο PEGMA (M_w = 475 g/mol) χρησιμοποιήθηκε σε αντιδράσεις συμπολυμερισμού μαζί με το παράγωγο της ντοπαμίνης (dopamine methacrylamide, DMA) ως συμμονομερές για τη σύνθεση PEGMA-*co*-DMA υδρογελών με φωτοεκκινητή το g-C_3N_4. Οι κατεχόλες του DMA συμμετείχαν στη διασταύρωση των πολυμερικών αλυσίδων μέσω δεσμών υδρογόνου, π-π stacking κ.ο.κ., οδηγώντας στην σύνθεση υδρογελών χωρίς την προσθήκη κάποιου επιπλέον διασταυρωτή. Οι υδρογέλες που συντέθηκαν έδειξαν ικανότητες προσρόφησης νερού (swelling) που εξαρτώνται από το βαθμό διασταύρωσης και εξαιρετικές τιμές swelling έως και 2000%.

1.Introduction

1.1 Overview of Tissue Engineering

Tissue Engineering (TE) and Regenerative Medicine (RM) are two interconnected and rapidly growing fields of research since their first proposed definition in 1988. According to the Handbook of Tissue Engineering Scaffolds[1], tissue engineering was primarily defined as "the application of the principles and methods of engineering and life sciences toward the fundamental understanding of structure-function relationships in normal and pathological mammalian tissue and the development of biological substitutes to restore, maintain, or improve tissue function". Regenerative Medicine has been similarly termed as a practice that aims at "replacing or regenerating human cells, tissues or organs, to restore or establish normal function"[2]. Owing to the success stories of the development of induced pluripotent stem cells, the breakthroughs in the development of biomaterial scaffolds and the arising of novel biofabrication techniques, TE and RM applications appear to have great potential of translation to everyday clinical practice.[3] In that sense, it is rather straightforward that the advances in this field require the conjugation of multiple research and engineering practices. The main pillars of progress in tissue engineering are cell, materials, and tissue architecture engineering[3] as they can be seen in Figure 1.1.

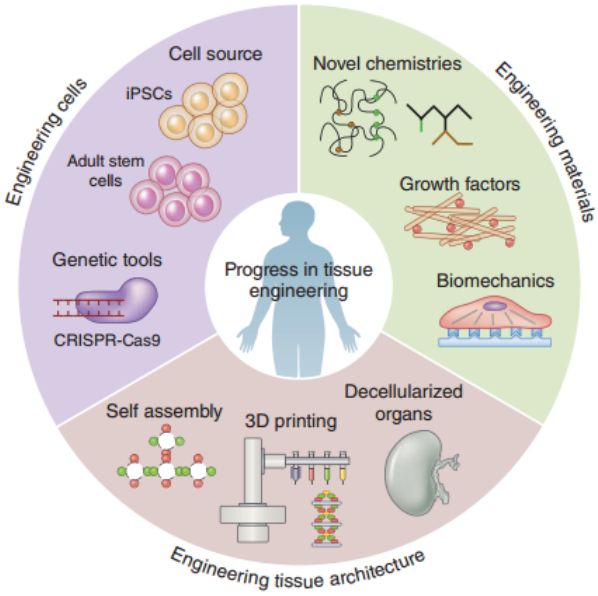

Figure 1.1 – The pillars of progress of Tissue Engineering[3]

In a more simplified manner, the aim of TE is to create novel therapeutic methodologies that will address the treatment of diseased, damaged, or degenerated tissue. Allografts and autografts have been the treatment of choice for many years, but they suffer from serious limitations. Autografts, meaning the transplantation of healthy tissue from another site to the diseased or damaged one in the same patient, can be costly, painful to the individual and sometimes dangerous as far as recovery of the tissue is concerned in both tissue sites. Allografts, which are taken from another individual and transplanted to the patient, suffer donor-patient compatibility limitations as well as unwanted infections. In both cases the availability of tissue is a concerning factor, to which tissue engineering offers a great solution via the production of artificial tissues. The three main elements that are essential to this process are cells, signals and scaffolds which are commonly referenced as a tissue engineering triad.[4]

1.2 Tissue Engineering Scaffolds

1.2.1 Tissue Engineering Scaffold Properties

Scaffolds in tissue engineering serve the role of a temporary "home" for the seeded cells, imitating the native extracellular matrix properties.[1] Independently of the tissue of application, the design of a scaffold must fulfill some prerequisites, namely biocompatibility, biodegradability and mechanical properties similar to the tissue ECM in question.[1,4,5]

Biocompatibility is one of the most important factors that should be taken into consideration when designing a scaffold. A material is referred to as a biomaterial or as biocompatible when it exhibits "the ability to perform with an appropriate host response in a specific situation", as it was described by David Franklin Williams in 1987[6]. In simple terms, in order for a material to be considered biocompatible it should be able to co-exist with live cells or surrounding tissue in a mutually acceptable manner, meaning causing a minimal to no immune response. For tissue engineering scaffolds that are usually in direct contact with live cells and tissues, cells should be able to sufficiently attach themselves on to the material, to make use of its functionalities to function properly, proliferate and migrate within the artificial matrix[1],

while at the same time the material should not be rejected by the human body and should exhibit low or no levels of toxicity and no tumorigenicity[7].

Biodegradability is another major aspect to be discussed concerning tissue engineering scaffolds since in principle the seeded cells or the native cells of the damage tissue site are supposed to regain the ability to produce their own matrix. This means that the scaffold should be able to degrade and be digested through enzymatic reactions in a time-sensitive manner giving up space for the newly produced ECM and at the same time providing the mechanical integrity needed for tissue to be constructed. Thus, apart from the scaffold material, its degradation byproducts should also exhibit biocompatibility and non-toxicity[1,4]

In terms of mechanical properties, as it has been already mentioned, the designed material should be able to provide the constructed tissue with mechanical integrity and stability and also imitate the local mechanical behavior of native extracellular matrix (load bearing, elastic modulus etc.). The scaffold material must match these dynamic requirements throughout the whole lifespan of the tissue engineering process, from biofabrication, to cell seeding, to tissue growth and permanent implantation and at last through metabolization.[4,8]

Another required property of tissue engineering scaffolds is biofunctionality, which can be introduced either by modifying the scaffolds with biological motifs that can be promoting of cell proliferation and tissue growth, or by functionalizing the scaffold so as to release growth factors essential for the support of tissue construction. Different stimuli can also be introduced to enhance the performance of the scaffold by tuning the architecture and the morphology, so as to provide mechanical stimulation or even employing stimuli responsive materials that will provide stimulation upon excitation. Finally, structural factors such as the dimensionality of the scaffold that can influence the direction of tissue growth or porosity that can enhance the permeation of nutrients should be considered. All of the above are summarized in Figure 1.2.

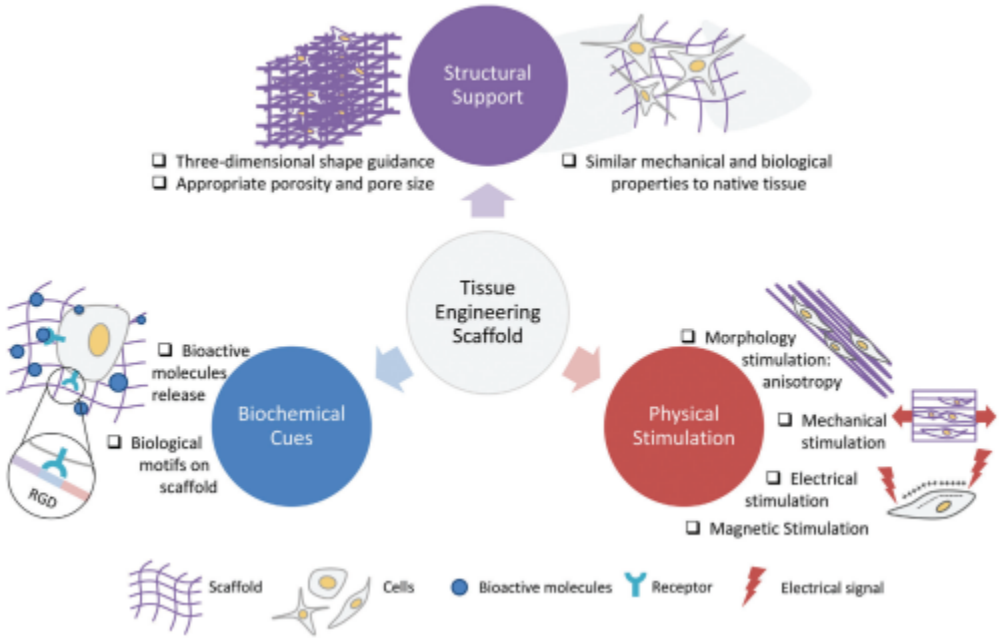

Figure 1.2 – Important factors in tissue engineering scaffold design[9]

1.2.2 Tissue Engineering Scaffold Materials

There is an abundance of materials that fit the requirements to be used in the preparation of tissue engineering scaffolds and they can be classified in three major classes. These are metals, ceramics and polymers. While metals and ceramics fall in the category of inorganic materials that have been widely used and investigated for their exceptional mechanical properties, polymers which are organic long chain macromolecules with a large number of repeat units, can be more versatile and tunable. Hybrids of those materials have also been proposed. [10]

Metals and alloys have been used for a long time in the medical field as implants to support the regeneration of hard tissue, like bone, as total joint replacements or even as stents. Owing to their metallic bonds, they are characterized by extreme mechanical strength and corrosion resistance that are both very desirable properties for this certain application. One of the main drawbacks of these materials is their possibly toxic byproducts, such as metal ions that can induce an inflammatory response, as well as stress

shielding due to their high mechanical moduli which can lead to atrophy of the newly constructed tissue.[10,11]

Ceramics have also been used as implantable materials for similar applications as those of metals. Bioactive glasses such as hydroxyapatite, calcium phosphates and other crystalline materials, such as alumina and zirconia are well-known biocompatible materials. Due to their exceptional mechanical properties, like high abrasive strength, but also to their porous structure that allows the permeation of nutrients, they have been extensively used as osteoconductive coatings for metal implants.[10,11]

Polymers can be classified, as either synthetic or natural based on their origin and as either degradable or non-degradable based on their biodegradation properties. Natural polymers, such as polypeptides, proteins, polysaccharides, and polynucleotides exhibit many advantageous properties such as great biocompatibility, biodegradability, bioactivity and non-toxicity. However, they suffer from limited processability, low degradation tunability and poor mechanical properties. On the other hand, synthetic polymers allow easier modification and reproducibility than natural polymers, alongside controlled degradation and tunability, but are inferior in terms of biocompatibility. Some of the most extensively studied natural and synthetic polymers are illustrated in Figure 1.3.[11,12]

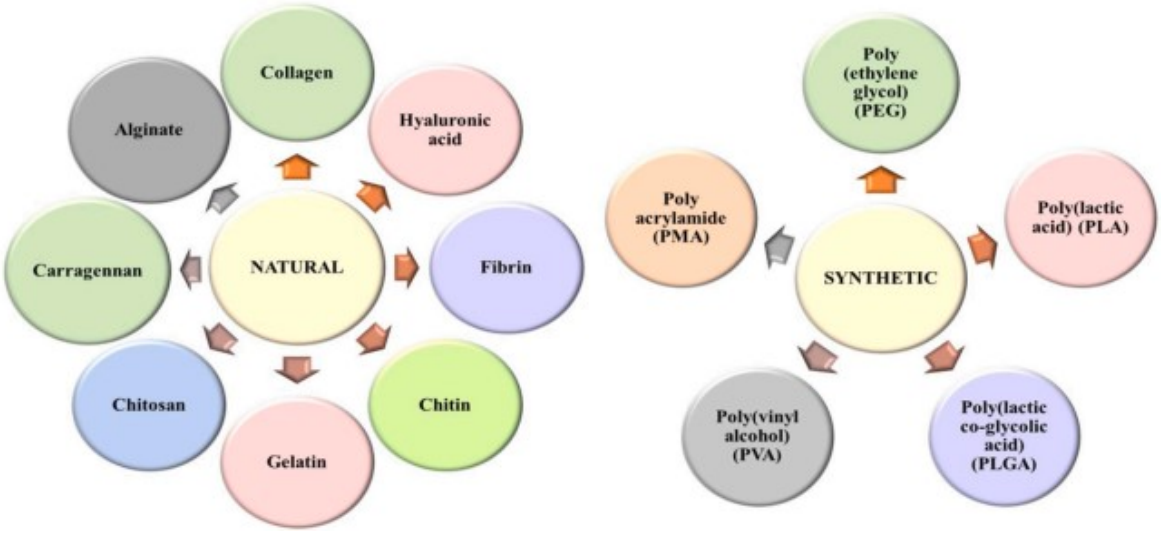

Figure 1.3 – Classification of polymer materials used in tissue engineering and honorable mentions.[13]

1.3 Hydrogels for Tissue Engineering

Hydrogels are a class of crosslinked hydrophilic polymers that have the ability of absorbing large quantities of water. They first emerged as promising materials for biological use in 1960 as proposed by Wichterle and Lim[14] and since then, they have been applied in many bio- and medicine related applications, such as contact lenses, biosensors, drug delivery carriers and also tissue engineering.[15] The wide recognition of hydrogels as potent tissue engineering materials resides in their exceptional properties, such as their high water content, excellent permeation of nutrients and cell encapsulation in 3D structures. The abundance of crosslinking mechanisms and methods available is the key to obtaining hydrogels with desired properties, namely gelation times, mechanical moduli etc.[5]

1.3.1 Photopolymerizable Hydrogels for Tissue Engineering

Photopolymerization is an advantageous technique that can be used for the preparation of hydrogels. The main advantage of the method lies in the spatiotemporal control of the process employing UV or visible light and fast crosslinking rates, ranging from seconds to minutes either in room or physiological temperature, producing minimal to no heat at all.[5,15] These processes require a specific type of initiator, called the photoinitiator, that can be excited by UV or visible light to produce radicals that can initiate and propagate the polymerization. The proper photoinitiator should fulfil similar prerequisites to those discussed for tissue engineering scaffolds, i.e. biocompatibility, stability and non-toxicity, as well as solubility in water.[15,16]

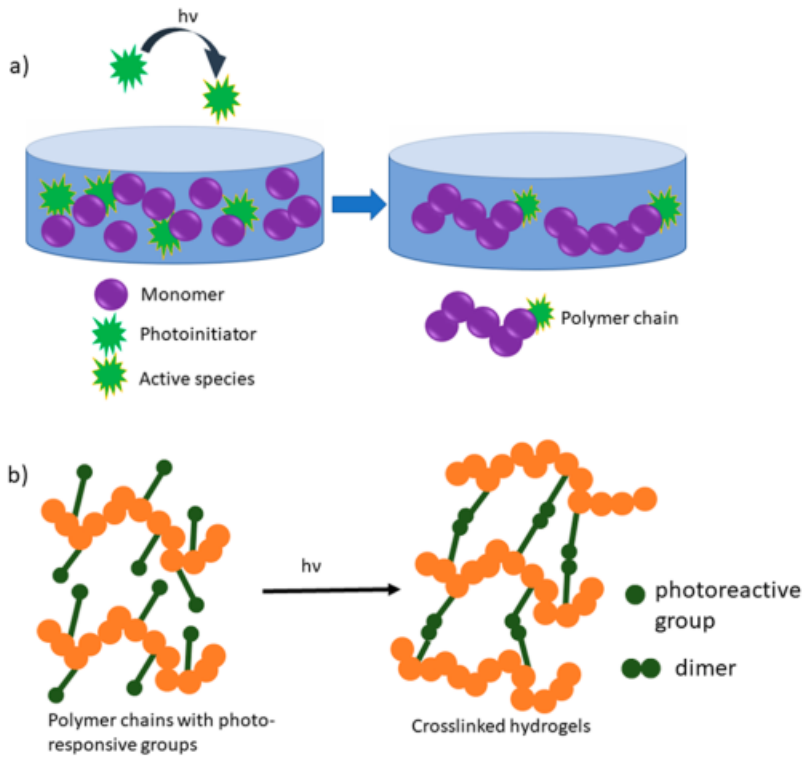

Figure 1.4 – (a) Photopolymerization and (b) photo crosslinking[17]

The most common photopolymerization reaction used in hydrogel synthesis is the free-radical-initiated chain polymerization. Important factors that can affect this reaction in terms of reaction rate and grafting density, are the photoinitiator type, as well as its concentration in the photopolymer solution, but also the duration of irradiation and the source intensity and wavelength. Photoinitiators that will create radicals are classified in two main classes. The Type I class comprises initiators that have cleavable bonds. Such families of materials have been reported in the literature to be benzoin and acetophenone derivatives that contain carbonyl groups. When light is absorbed by these materials, they can undergo a process called α-cleavage, which is the homolytic cleavage of their α-carbon bonds to produce two radical species. The Type II photoinitiator class contains initiators that upon light irradiation and absorption will be led to an excited state, from which they cannot automatically produce radicals but need a co-initiator to perform hydrogen abstraction or electron transfer. Aromatic ketones such as benzophenone and thioxane are

considered as Type II photoinitiators and tertiary amines, alcohols, ethers and thiols are the most commonly used co-initiators.[15,17,18]

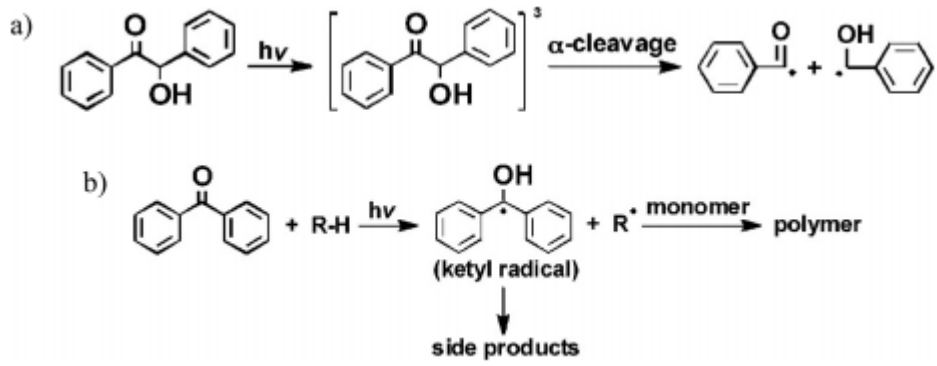

Figure 1.5 - Photoinitiator mechanisms of action: Type I (a) Photoinitiation via α-cleavage and Type II (b) Photoinitiation via H-abstraction[17]

The type of monomers that are photocurable and photocrosslinkable via this radical process are also specific. Acrylate bearing monomers have been widely reported in UV curable resins, as well as vinyl ethers.[19] Several acrylate functionalized natural polymers have been reported in literature to have been used in photopolymerizable hydrogels for tissue engineering applications, with gelatin, chitosan, alginate and cellulose being predominant.[17]

1.4 g-C_3N_4 as a novel photoinitiator

Graphitic carbon nitride (g-C_3N_4) is a semiconducting carbon based material that has been extensively studied in the field of photocatalysis owing to its special properties and its ability to perform water splitting under visible light irradiation that was reported by Wang et al. back in 2009 [20]. Although the first references to polymeric carbon nitride date back to 1834, newly found interest has been expressed in recent years as the photoinitiating and photocrosslinking properties of the material were explored.[21–23]

Synthesis of g-C_3N_4 can be achieved through various methods. One of the most popular methods is the thermal polycondensation of low molecular weight nitrogen-rich organic precursors, such as urea, dicyanamide, thiourea and melamine, at high temperatures.[24] The final properties of the obtained material depend on the precursors utilized as well as the duration and temperature of the polycondensation.[25] The

synthetic route from melamine to carbon nitride and its physicochemical characterization are depicted in Figure 1.6

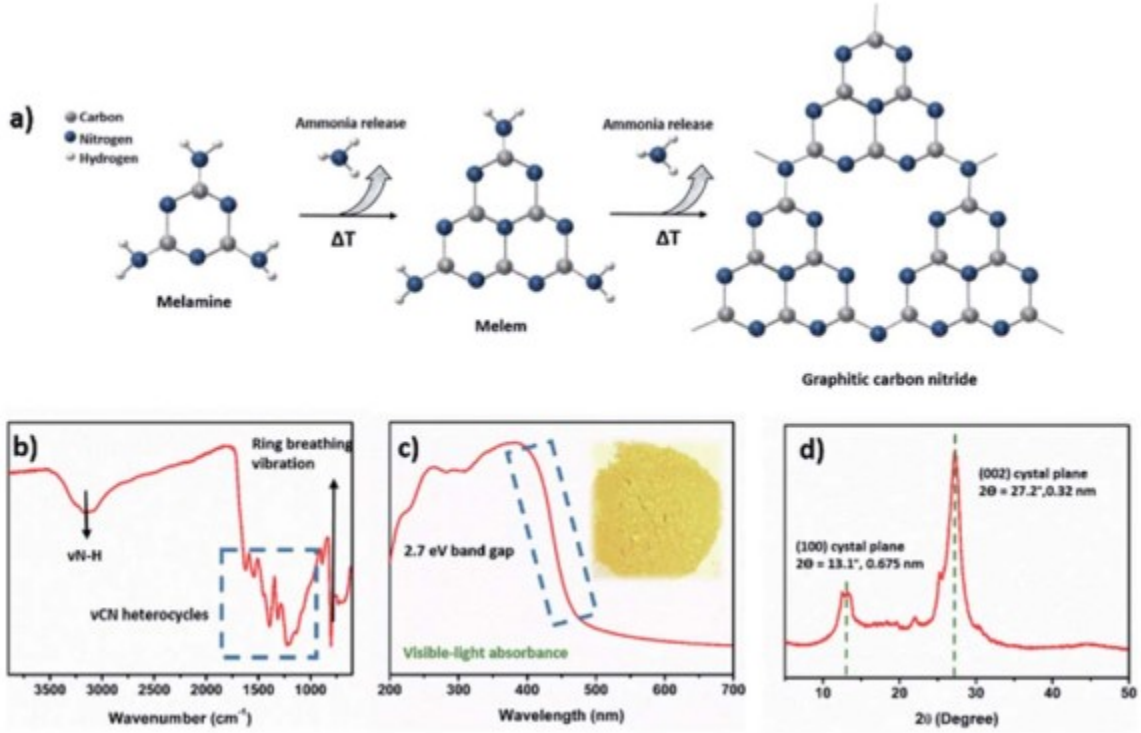

Figure 1.6 – (a) Synthetic route from melamine to g-C_3N_4. **(b)** FT-IR, **(c)** UV-Vis and **(d)** XRD spectra of g-C_3N_4 powder.[25]

Allotropes of g-C_3N_4 of different dimensionalities like quantum dots, nanotubes and nanosheets have been reported in literature.[24] g-C_3N_4 nanosheets have a 2D architecture and can be obtained from bulk g-C_3N_4 through exfoliation, either thermal or liquid.[24]

Recently, g-C_3N_4 in the form of nanosheets has been employed as photoinitiator in free radical polymerization of hydrogels[26–28] for various applications. The underlying mechanism of photoinitiated polymerization to obtain hydrogels from water solutions is presented in Figure 1.7. Under visible light illumination, g-C_3N_4 nanosheets can be excited leading to generation of electron-hole pairs that can be involved in OH radical formation.[27]

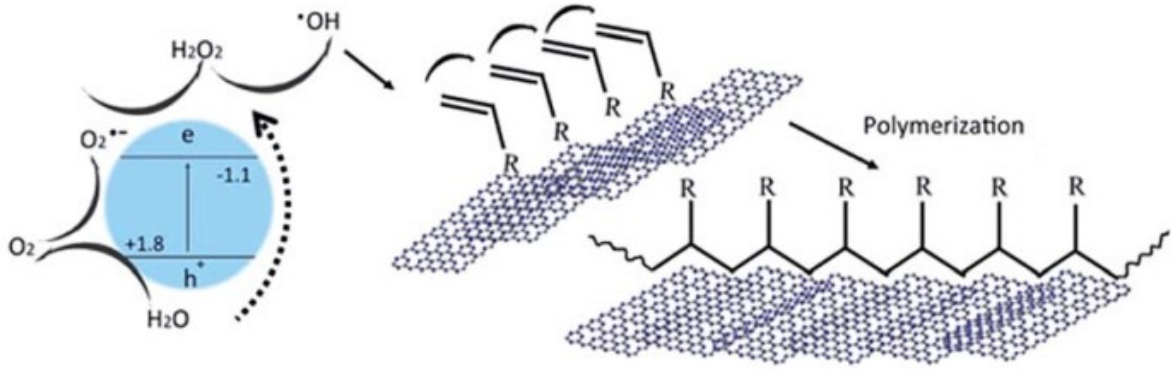

Figure 1.7 – Possible steps of the photoinduced hydrogelation through photocatalytic generation of hydroxyl radicals in water.[27]

1.5 Aim of this thesis

g-C_3N_4 nanosheets have been reportedly used in various bioapplications[29–33], predominantly as bioimaging agents[29,30]. However, g-C_3N_4 excellent visible light photoinitiating properties and green chemistry have not been exploited for biomedical applications yet. This thesis aims at the synthesis of novel photopolymerizable hydrogels, that will be used as scaffolds for tissue engineering, via the incorporation of g-C_3N_4 as a novel photoinitiator.

To achieve this, three different photopolymerizable derivatives of natural origin were synthesized namely dopamine methacrylamide, gelatin methacrylamide and alginate methacrylate, to be used as comonomers in the free radical photopolymerization. Here, the preliminary synthesis of hydrogels using one of these monomers, dopamine methacrylamide, to copolymerize it with commercially available PEGMA (M_w=475 g/mol) using g-C_3N_4 synthesized in our lab as the photoinitiator in the presence of ethylene glycol dimethacrylate as a crosslinker, is introduced. The results of a second series of experiments without incorporating the crosslinker to obtain hydrogels and the swelling profiles of all synthesized hydrogels are presented.

2. Materials and Methods

2.1. Materials

2.1.1. Materials used for Synthesis

Dopamine Hydrochloride and Melamine, where purchased from Alfa Aesar. Alginic Acid Sodium Salt, Glycidyl Methacrylate, Methacrylic Anhydride, Poly(ethylene glycol) methyl ether methacrylate (PEGMA, M_w = 475 g/mol) and Sodium Tetraborate, where provided by Aldrich. PBS tablets and Gelatin from Bovine Skin were supplied by Sigma, while ethylene glycol Dimethacrylate (EGDMA) by Merck. Before use, PEGMA was passed through a basic alumina column to remove the inhibitor. Sodium hydroxide pellets were obtained from Panreac, and Sodium bicarbonate was purchased from Sigma Aldrich. Hydrochloric Acid was purchased from Scharlau.

2.1.2. Materials used for Cell Cultures

Trypsin/EDTA (0.25%), phosphate buffer saline (PBS), Amphotericin-B (fungizone), L-glutamine, penicillin/streptomycin (P/S), were all purchased from Gibco ThermoFisher Scientific. PrestoBlue™ reagent for cell viability and proliferation was obtained from Invitrogen Life Technologies and also Minimum essential Eagle's medium (α-MEM) was specifically used for the Cell Culture of MC3T3-E1 cells.

2.2. Methods

2.2.1. Synthesis of Bulk g-C_3N_4

Bulk g-C_3N_4 was synthesized by thermal polycondensation of melamine as proposed by Yan et al.[34]. 4 g of melamine were placed in closed crucibles and were heated at 550ºC for 4 h with a heating rate of 5ºC/min. The resulting yellow powder was repeatedly washed with milliQ water, was collected by centrifugation and dried under vacuum overnight.

2.2.2. Synthesis of Exfoliated g-C_3N_4

Exfoliated g-C_3N_4 was prepared by the thermal exfoliation of bulk g-C_3N_4 as suggested by Niu et al. [35]. In specific, 3.25 g of bulk g-C_3N_4 was heated in open crucibles at 550ºC for 4 h with a heating rate of 5ºC/min.

2.2.3. Preparation of g-C_3N_4 Nanosheets

g-C_3N_4 Nanosheets were obtained by sonicating 700 mg of the thermally exfoliated g-C_3N_4 in 70 mL milliQ water, for 4 h. The milk-like dispersion was subsequently centrifuged at 3000 rpm for 10 min, the supernatant was kept while the precipitate containing larger, non-exfoliated sheets was discarded. The retrieved supernatant was centrifuged at 11000 rpm for 30 min to collect the g-C_3N_4 Nanosheets and the precipitate was recovered and redispersed in 10 g of milliQ water, yielding a dispersion with a concentration of 5 mg/g.

2.2.4. Synthesis of DMA

Synthesis of Dopamine Methacrylamide (DMA) was done following a method proposed by P. Glass et al.[36]. Briefly, the reaction medium was prepared by dissolving 5 g of sodium tetraborate and 2 g of sodium bicarbonate in 50 mL of milliQ water in a three-necked spherical flask. The mixture was degassed with nitrogen for 10 min. Afterwards 2,5 g of dopamine hydrochloride were added under stirring, and the mixture was again degassed for a few minutes.

In a separate vial, 2,55 mL of methacrylic anhydride and 12,5 mL of THF were added under stirring and subsequently degassed for another 10 min. Then the mixture was transferred with a syringe into the reaction flask. The pH of the resulting solution was maintained at pH~8 using 1M NaOH solution. The reaction was allowed to continue overnight.

Next, the solution was washed two times with 25 mL of ethyl acetate and then filtered. The pH of the filtrate was adjusted at ~2 adding a 6M HCl solution under stirring. The organic layer of the solution was then extracted three times using 30 mL ethyl acetate. After extraction, the organic layer was dried over $MgSO_4$. The solution was filtered, precipitated in hexane, and refrigerated for 1 h in order to promote the

formation of crystals. The supernatant was discarded, and the precipitate was dried under vacuum overnight. The resulting material was collected as a white crystal powder.

The successful synthesis of DMA was confirmed via H^1-NMR analysis.

2.2.5. Synthesis of GelMA

The synthesis of Gelatin Methacrylamide (GelMA) was done according to the proposed method by Van den Bulcke[37] . In a spherical flask a solution 5 w/v% of gelatin in PBS was prepared under stirring at 50ºC. After complete dissolution of gelatin to a clear light brown solution, methacrylic anhydride was added to the solution following different ratios, which can be seen in the Table 2.1, in order to achieve different degrees of modification. The reaction was allowed to proceed for 3 h, after which the solution was transferred to a 3.5 kDa dialysis membrane and was dialyzed against milliQ water at 40ºC for 7d to remove any unreacted methacrylic anhydride and its byproducts. After purification the product was freeze-dried and stored at 4ºC until further use.

The modification and degree of modification with methacrylic units were confirmed and drawn out of H^1-NMR spectrum analysis.

Table 2.1

Sample	Ratio of mL of methacrylic anhydride to g of gelatin
GelMA I	0.1:1
GelMA II	0.2:1

2.2.6. Synthesis of AlgMA

The synthesis of Alginate Methacrylate (AlgMA) was performed following the experimental procedure published by D.S. Lima et al.[38]. 100 ml milliQ water were added in a spherical flask and subsequently 1g of alginic acid sodium salt was added under stirring. After complete dissolution, the pH was adjusted at pH~3,5 using 1M aqueous solution of HCl and then the reaction flask was transferred in an oil bath at

60ºC. Under stirring, 0.65 mL of glycidyl methacrylate were added into the reaction medium and the reaction was allowed to proceed overnight.

The next day, the solution was collected, was precipitated in acetone and was filtrated. The white slurry that formed on the filter paper was then transferred into a beaker and was dissolved in 30 mL of milliQ water under stirring overnight. The next day, the product was freeze dried and stored at 4ºC until further use.

The modification with methacrylate groups was confirmed via H1-NMR analysis.

2.2.7. Hydrogel Synthesis

2.2.7.1 P(PEGMA-*co*-DMA) hydrogels with EGDMA as the crosslinker

For the synthesis of the P(PEGMA-*co*-DMA) hydrogel, with EGDMA as the crosslinker and exfoliated g-C_3N_4 as the photoinitiator, 5 different mole ratios between the two monomers were investigated, namely 0%, 2%, 5%, 10% and 20% mole ratio of DMA to PEGMA. In each case, the mass of the crosslinker added was 5 wt% to the total mass of monomers and the concentrations of PEGMA and g-C_3N_4 were kept constant for all gels, at 33.3 wt% and 0.3 wt% respectively. The reaction conditions are summarized in Table 2.2.

First, in 20 mL vials, 1 mg of the photoinitiator g-C_3N_4 was dispersed in 1 g of milliQ water and 1 g of ethylene glycol and then the vial was sonicated for 1 hour to achieve a stable dispersion. Afterwards, 1g of PEGMA was added, along with the respective amounts of DMA and EGDMA. After the complete dissolution of DMA under stirring, each vial was closed with a rubber septum and was degassed with nitrogen for 10 min. Finally, all solutions were photocured with a 365 nm UV lamp, until complete gelation.

Table 2.2

Sample	PEGMA wt%	g-C_3N_4 wt%	DMA moles% to PEGMA	EGDMA wt% to total mass of monomers
gel0	33.3	0.3	0	5
gel2	33.3	0.3	2	5
gel5	33.3	0.3	5	5
gel10	33.3	0.3	10	5
gel20	33.3	0.3	20	5

Each gel was subsequently washed with DMSO and with milliQ water for 2 days to remove any unreacted reagents. Finally, each gel was freeze-dried and stored until further use.

2.2.7.2 P(PEGMA-*co*-DMA) hydrogels without the EGDMA crosslinker

For the P(PEGMA-*co*-DMA) hydrogel synthesis without the EGDMA crosslinker, 2 different molar ratios between the two comonomers where investigated, namely 5% and 20% mole ratio of DMA to PEGMA. The concentrations of PEGMA and g-C_3N_4 were kept constant for both gels at 33.3 wt% and 0.3 wt% respectively (Table 2.3).

The protocol and the reaction conditions followed were similar to the previous synthesis.

Table 2.3

Sample	PEGMA wt%	g-C_3N_4 wt%	DMA moles% to PEGMA
gel5wc	33.3	0.3	5
gel20wc	33.3	0.3	20

2.3. Characterization

Field Emission Scanning Electron Microscopy (FE-SEM, JEOL JSM-7000F) was employed for the observation of the morphology of the bulk, the exfoliated and the g-C_3N_4 nanosheets. Samples were prepared by dispersing the powder samples in 2-propanol via vortexing and sonication and drop-casting on glass substrates. Similarly, a small amount of the nanosheet dispersion was diluted with 2-propanol and was drop-casted on a glass substrate. After overnight evaporation of the solvents at room temperature, all samples were sputtered with a thin layer of Au.

X Ray Diffraction (XRD) patterns were recorded for bulk and exfoliated g-C_3N_4 with a PANalytical Xpert Pro X-ray diffractometer, using Cu K_α radiation (45kVand 20 mA). Diffuse Reflectance UV-Vis measurements were measured on a Shimadzu UV-2401 PC spectrometer equipped with an ISR-240A integrating sphere, using $BaSO_4$ as a total reflectance standard. Fourier transform infrared (FT-IR) spectra were recorded by a Thermo Scientific Nicolet 6700 spectrometer using powder samples of the bulk and exfoliated g-C_3N_4.

H^1 NMR Spectra of DMA, GelMA and AlgMA and the precursors Gelatin and Alginic Acid Sodium Salt were recorded on a Bruker AMX-500 NMR spectrometer. The DMA ^1H NMR sample was prepared by dissolving DMA in $(CD_3)_2SO$. GelMA and AlgMA samples and their precursors were prepared with D_2O as a solvent and the respective spectra were recorded at 50ºC.

2.4. Cell Culture Experiments

The cell culture experiments were conducted by Mrs. Danai Papadogianni in the Biomaterials for Tissue Engineering Lab of the Materials Science and Technology Department of the University of Crete. The cytocompatibility assessment experiments for bulk g-C_3N_4 and g-C_3N_4 nanosheets on adherent cell lines of mouse osteoblasts (MC3T3-E1). Cell culture conditions were set at 37ºC, under 5% CO_2 atmosphere, and the cell culture media of choice was Minimum essential Eagle's medium (α-MEM).

For the cell viability measurements, the PrestoBlue™ reagent protocol was employed. Briefly, 5000 cells/well were seeded in a 96-well plate overnight. Then they were incubated with 1 μgmL^{-1}, 3,75 μgmL^{-1}, 6,25 μgmL^{-1}, 12,5 μgmL^{-1}, 25 μgmL^{-1}, 50 μgmL^{-1}, 100 μgmL^{-1}, 300 μgmL^{-1} concentrations of the g-C_3N_4 materials for 48h in quadruplicates. Afterwards the supernatant from each well was removed and replaced with 150μL of 1:10 of Presto Blue Solution in Medium. The cells were incubated again in dark conditions for 1h and afterwards the supernatant was collected and transferred to a new 96-well plate to measure the absorbance at 570 and 600 nm in a Synergy HTX Multi-Mode Microplate Reader.

2.5 Swelling Degree of Hydrogels

Swelling studies were performed with the gel20, gel10, gel5 and gel20wc and gel5wc samples to assess the swelling behavior of the gels.

in PBS. Each vial containing the gel was filled with PBS up to the top of the vial and at specific time points for gel20, gel10 and gel20wc, the gel was retrieved from the buffer, blotted with paper, and then weighted. For gel5 and gel5wc the measurements were done by decanting the respective buffers in beakers and measuring the total mass of the vials with the swelled gels inside. After each measurement the respective buffer was transferred again in the vials.

In all cases the swelling degree was calculated according to the following equation

$$Swelling\ Degree = \frac{W_{swollen} - W_{dry}}{W_{dry}}$$

3. Results and Discussion

3.1 Synthesis and Characterization of g-C_3N_4

Bulk g-C_3N_4 was synthesized by the thermal polycondensation of melamine, as seen in Scheme 3.1. In specific, at high temperatures ammonia is eliminated and through rearrangement, tri-s-triazine groups are formed which at even more elevated temperatures, i.e. over 520ºC, condensate to the polymeric structure of C_3N_4[25,39].

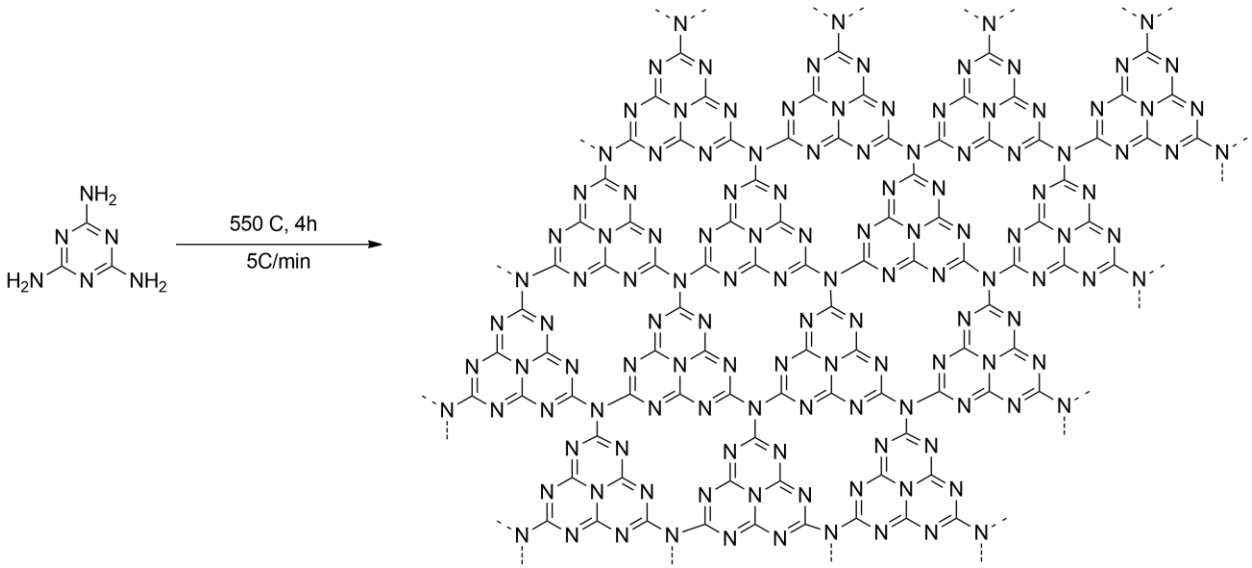

Scheme 3.1. Thermal polycondensation reaction of melamine

Subsequent thermal exfoliation was performed to derive the exfoliated g-C_3N_4 and then a liquid exfoliation in water via ultrasonication for 4 hours was performed on the previously thermally exfoliated product to obtain g-C_3N_4 nanosheets.

3.1.2 Physicochemical and Structural Characterization of g-C_3N_4

FT-IR spectra and XRD pattern of both the bulk and the exfoliated material can be found in Figure 3.1. Diffuse Reflectance UV Spectroscopy measurements were also performed and analyzed for both materials to calculate their photonic bandgap and are presented in Figure 3.2.

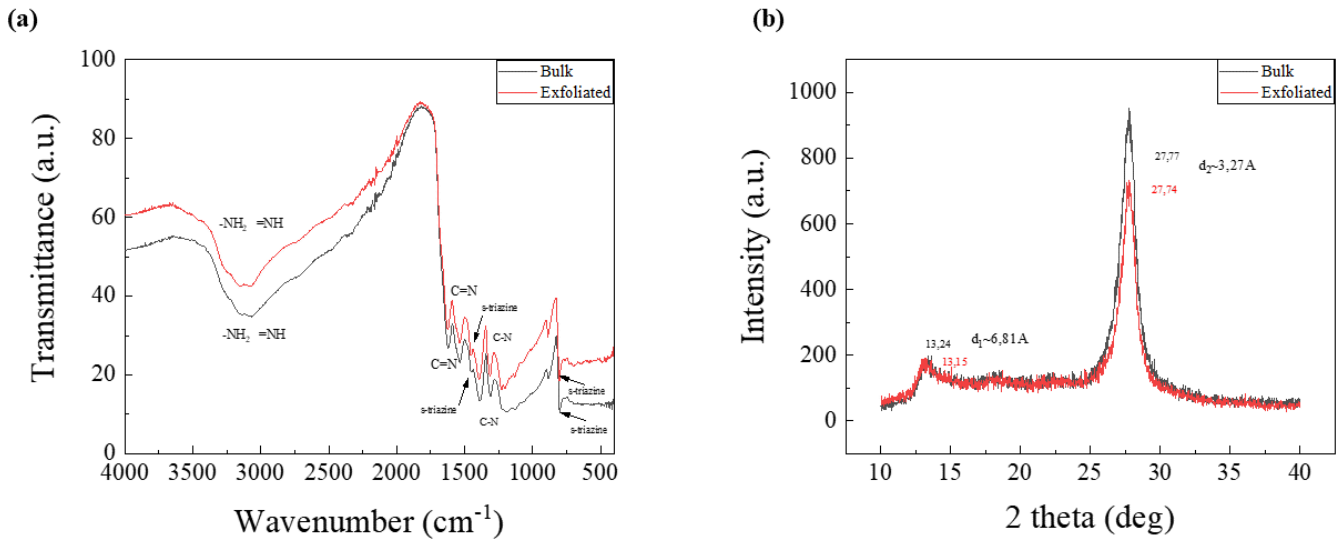

Figure 3.1. (a) FT-IR spectra and **(b)** XRD pattern of bulk and exfoliated g-C_3N_4.

The FT-IR spectra of the two materials (Figure 3.1a) are very similar. For the bulk material, the characteristic peaks of the s-triazine ring modes appear at 802 cm^{-1} and 1450cm^{-1} alongside with the C-N and C=N stretching modes at 1311 cm^{-1} and 1621 cm^{-1}, respectively. For the exfoliated product, the s-triazine ring modes are formed at 804 cm^{-1} and 1452 $cm^{-1,}$ while the C-N and C=N stretching modes at 1313 cm^{-1} and 1625 cm^{-1}. In both spectra a broad band appears for the -NH_2 and -NH terminal groups in the range of 3000 to 3500 cm^{-1}.

In the XRD patterns of the bulk and exfoliated material (Figure 3.1b) two distinct peaks can be observed. The diffraction peaks at 13.15° and 13.24°, for the exfoliated and the bulk g-C_3N_4, respectively, corresponds to the planar structural stacking and to a characteristic distance d_1 approximately equal to 6,81 A, for both materials, while the second peak at 27.74° and 27.77° appears due to the interlayer stacking and a computed interlayer distance d_2 of 3.27 A.

Diffuse Reflectance UV measurements for both materials revealed a strong absorption in the low visible region. More specifically, based on the Kubelka-Munk plots that were derived from the measurements, both the bulk and the exfoliated material exhibit a photonic bandgap of approximately 2.72 eV and an approximate excitation wavelength of 456 nm.

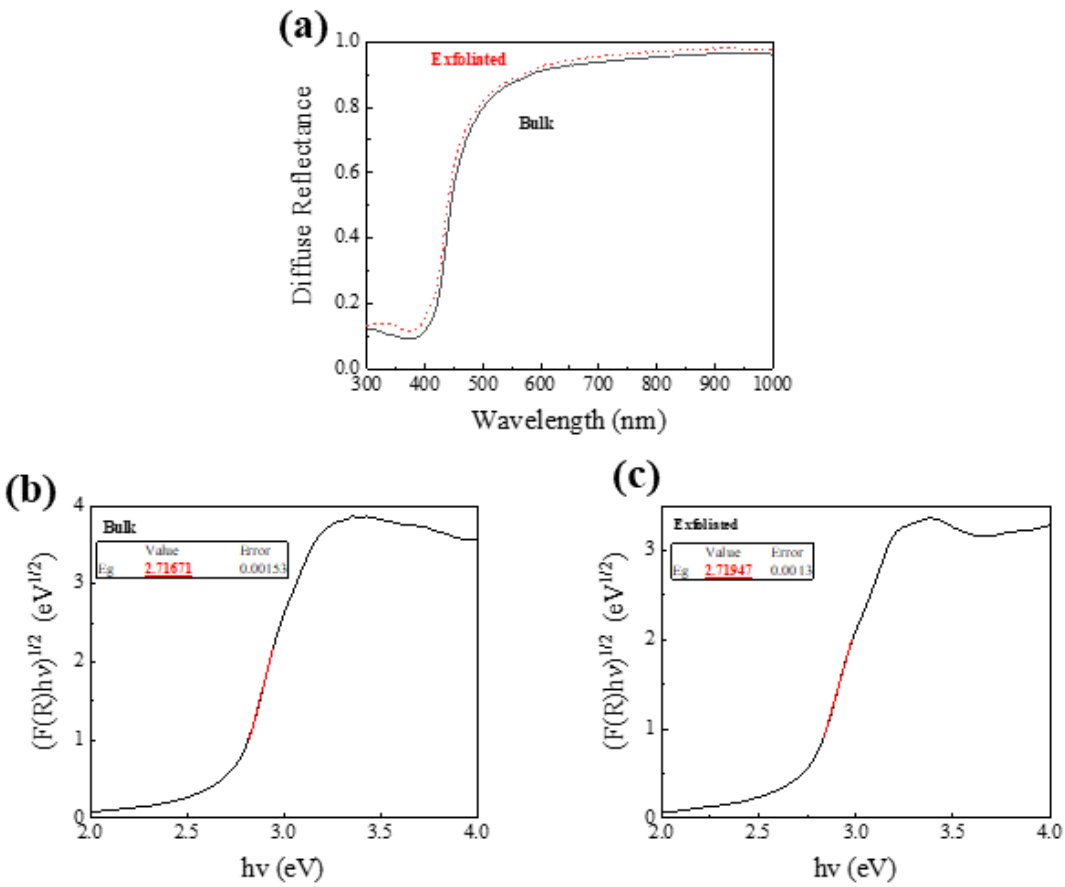

Figure 3.2. (a) Diffuse Reflectance Spectra of bulk and exfoliated g-C_3N_4 and their respective Kubelka - Munk plots **(b, c)**.

The main reason these characteristic measurements did not reveal significant differences between the bulk and the thermally exfoliated material, is probably due to the low exfoliation efficiency of the thermal process, resulting in the presence of stacked layers even in the exfoliated material. As it can be observed from the FE-SEM images obtained for the g-C_3N_4 samples (Figure 3.3), the bulk material appears to have an irregular, stacked structure in (a) and (b), the exfoliated material consists of shear sheets covering some of the remnants of the crystals of the bulk material in (c) and (d). However, in the case of the nanosheets

(Figure 3.3 (e) and (f)) the formation of nanosheets of small lateral size can be clearly observed. It is important to mention that usually the thicknesses of the obtained exfoliated materials reported in the literature are several times bigger than the reported interlayer distance of the stacked layers[24,29,40], except if the exfoliation is performed in presence of strong chemicals[41], which in our case could unfavorably interfere with the biocompatibility of the materials.

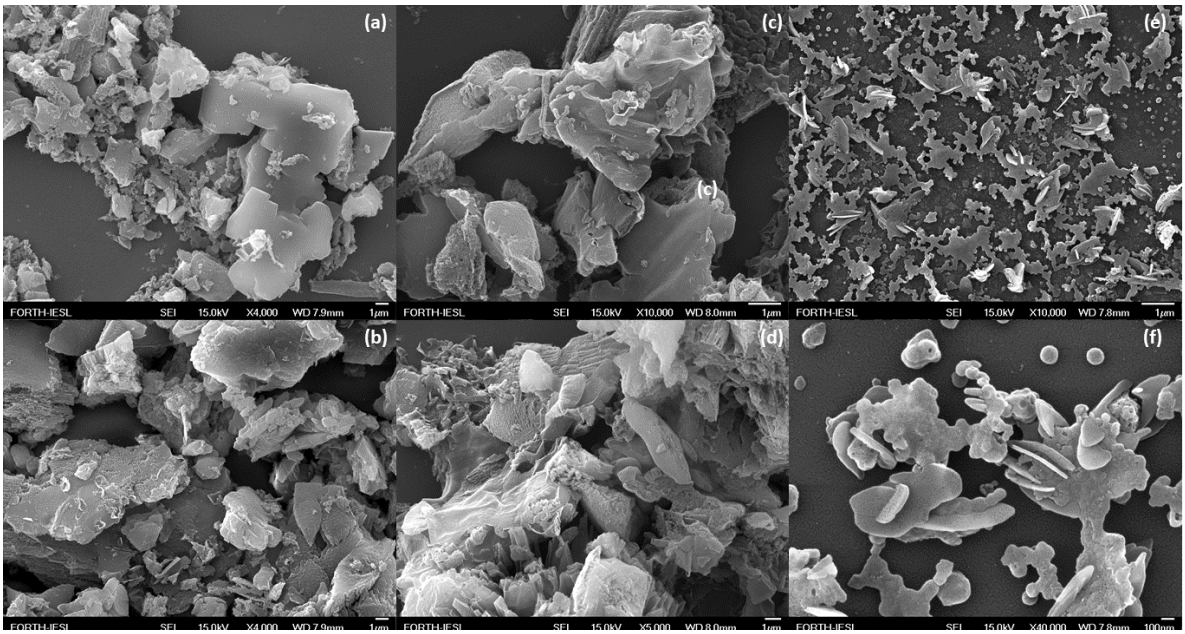

Figure 3.3. FE-SEM images of g-C_3N_4 in the forms of bulk **(a)**, **(b)**, thermally exfoliated **(c)**, **(d)** and nanosheets **(e)**, **(f)**.

3.1.3 g-C_3N_4 cytocompatibility experiments

Cytotoxicity assessment of bulk g-C_3N_4 and g-C_3N_4 nanosheets was performed in the Biomaterials for Tissue Engineering Lab by Mrs. Danai Papadogianni by employing the Presto Blue Cell Viability Assay. The mouse osteoblast cell line MC3T3-E1 was incubated with different concentrations of both materials for 48 hours with the cell culture conditions being set at 37ºC and 5% CO_2. The concentrations of the materials, as well as the duration of the experiment were carefully planned to match similar experiments documented in the bibliography[29,30,42].

The concentration dependent viability of the MC3T3-E1 cells over a 48h period can be seen in Figure 3.6. For the bulk material, a 60 % to 70% viability is observed while for the nanosheets a wider range of 55% to 75% viability is exhibited, both in comparison with the behavior and viability of the cells on the TCPS. In both cases the materials, although well dispersed in the medium, seemed to precipitate over the cells after the 48h period of time thus inducing this response that is within the appropriate limits of cell viability.

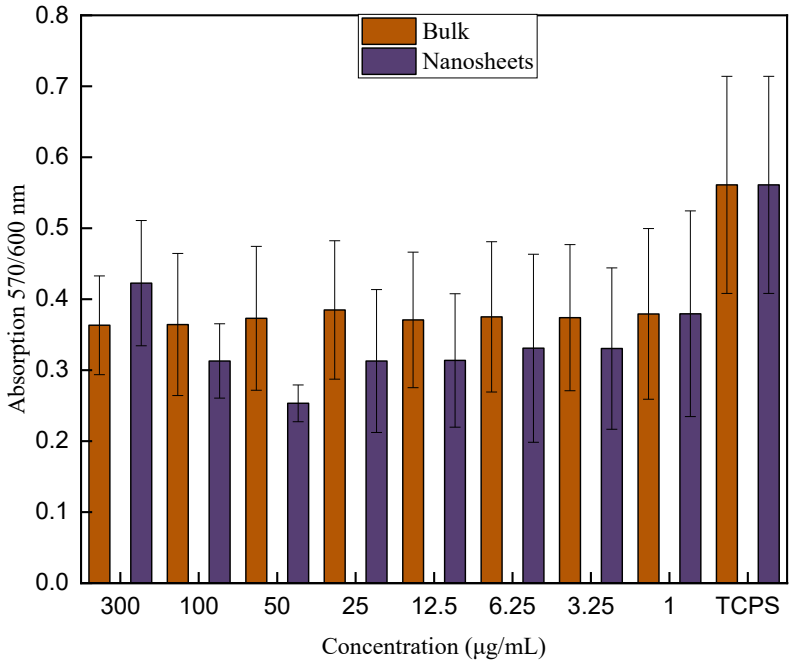

Figure 3.6. Cytocompatibility assessment of bulk g-C_3N_4 and g-C_3N_4 nanosheets of different concentrations measuring the metabolic activity of MC3T3-E1 in absorbance units.

3.2 Synthesis and Characterization of the Different Monomers

3.2.1 Synthesis and H[1]-NMR analysis of DMA

Dopamine methacylamide was synthesized by the reaction of dopamine hydrochloride with methacrylic anhydride according to a method provided in literature[36]. The reaction was done in saturated $Na_2B_4O_7$ and $NaHCO_3$ water medium to protect the catechol group.

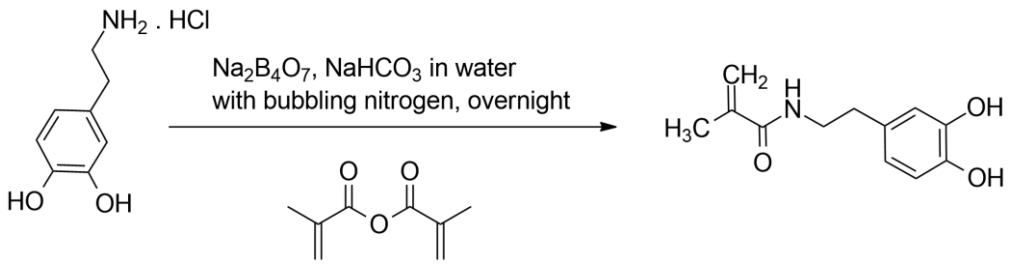

Scheme 3.2. Dopamine methacrylamide synthesis reaction

The successful synthesis was confirmed via H[1]-NMR spectroscopy and the respective spectrum is presented in Figure 3.4.

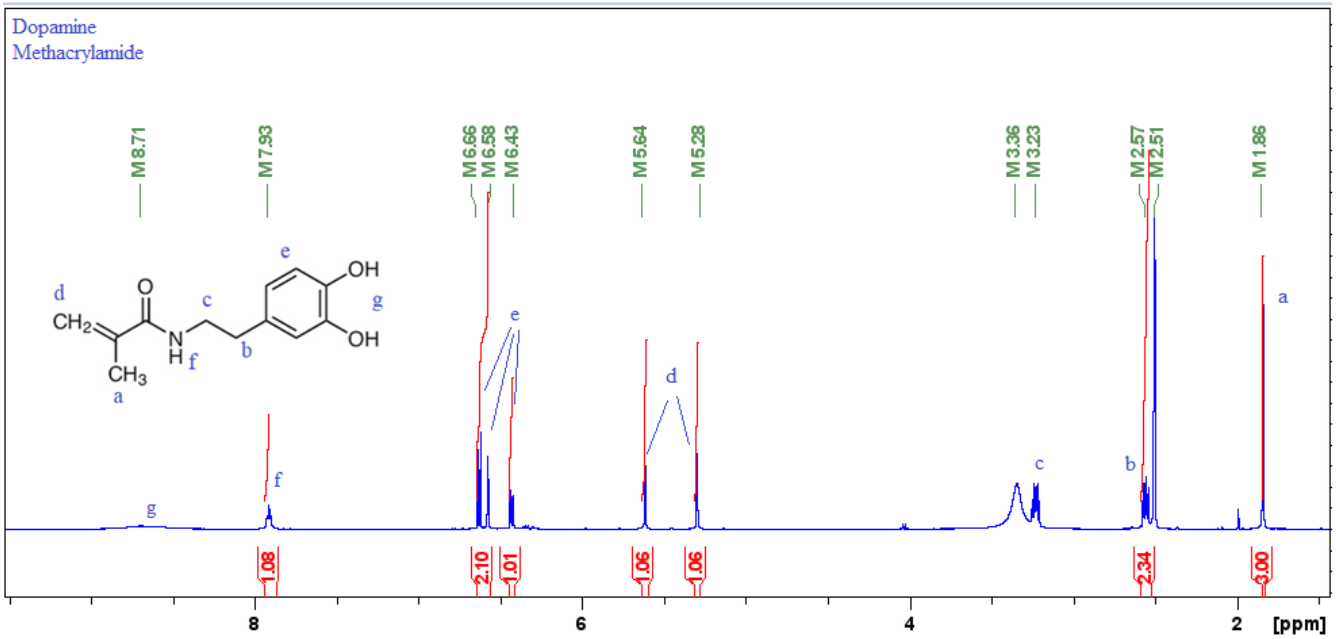

Figure 3.4. ^{1}H-NMR spectrum of Dopamine Methacrylamide in $(CD_3)_2SO$.

The two characteristic peaks of the protons of the double bond of the methacrylic units can be observed at 5.28 ppm and 5.64 ppm while the assignment and the integration of all peaks are in good agreement with the chemical structure of DMA verifying the successful synthesis of the monomer.

3.2.2 Synthesis and^{1}H- NMR analysis of GelMA

Gelatin methacrylamide was obtaining from reacting gelatin with methacrylic anhydride in PBS, at 50ºC, for 3 hours, following a method previously reported in literature[37]. The modification is suggested to take place on the amino, hydroxyl and/or carboxylic acid residues on the side chains of the amino acids, that for gelatin can be found on lysine and hydroxylysine, proline and hydroxyproline and on aspartic acid[43].

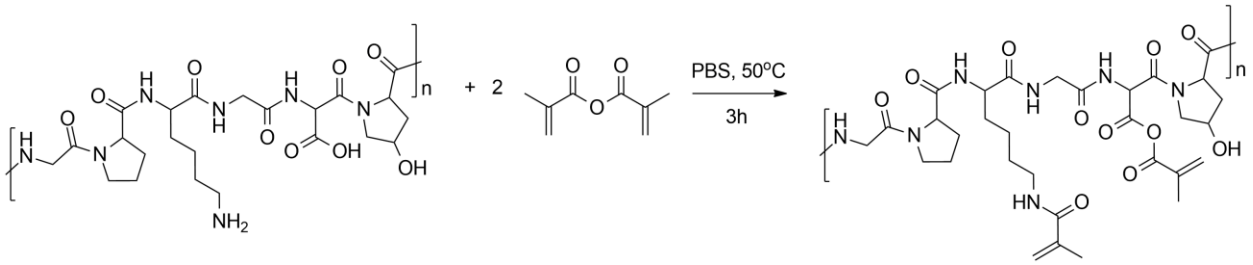

Scheme 3.3 – Gelatin methacrylamide synthesis reaction

The methacrylation of gelatin was confirmed by the appearance of two new peaks in the H^{1}-NMR spectra of the products which are presented in Figure 3.5

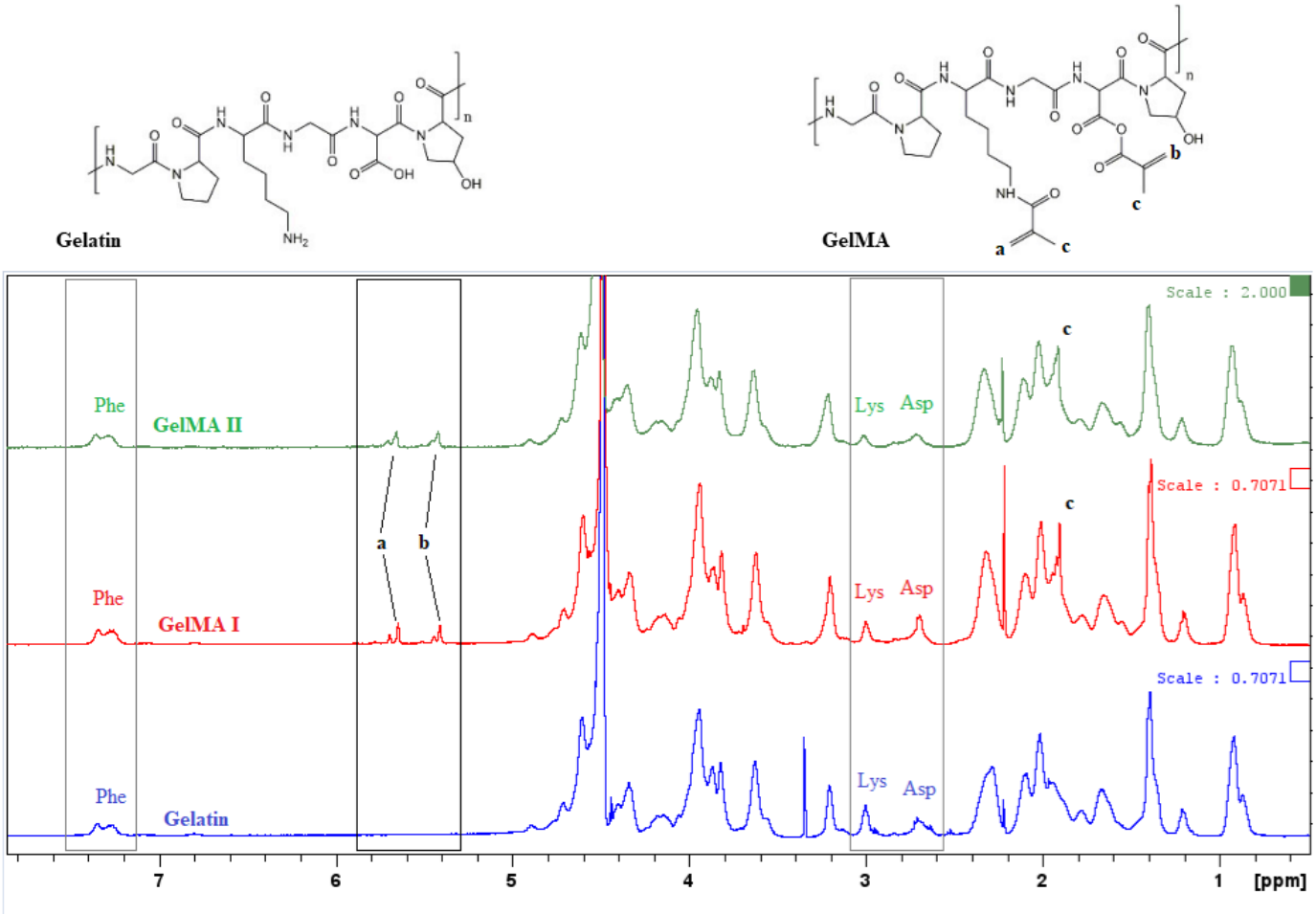

Figure 3.5. ^{1}H-NMR spectra of Gelatin Methacrylamide products and Gelatin, at 50ºC, in D_2O.

The peaks corresponding to the resonance of the amino acid sequence present in gelatin are prominent in all structures and correspond well to the ^{1}H-NMR analysis reported in the bibliography [44,45]. The appearance of two new distinct peaks at 5.40 and 5.65 for GelMA I and 5.42 and 5.65 for GelMA II correspond to the methylene protons of the methacrylic unit, while the 1.91 ppm peak intensity increases in both spectra due to the methyl protons of the group.

The degree of methacrylation for each functionalized product was calculated by comparing the integrals of the peaks of lysine and aspartic acid residues, that appear at around 3.00 and 2.72 ppm respectively, to the constant integral of the phenylalanine protons at 7.3 ppm. The integration results are summarized in Table 3.1.

Table 3.1

Sample	Phe Integral (I_1)	Lys Integral (I_2)	Asp Integral (I_3)	DoM Lys	DoM Asp	Average DoM
Gelatin	5	3.58	3.98			
GelMA I	5	2.79	2.78	22.07%	30.15%	26.1%
GelMA II	5	1.83	2.40	48.88%	39.69%	44.3%

The two products, GelMA I and GelMA II exhibit an average degree of modification of 26.1% and 44.3%. This is in agreement with the method of preparation of both materials as described in paragraph 2.2.5, were the ratio of methacrylic anhydride to gelatin is doubled for GelMA II with respect to the proportions used to synthesize GelMA I, yielding a degree of modification 1.7 times higher for the former.

3.3 Synthesis and ^{1}H-NMR analysis of AlgMA

Alginate Methacrylate was obtained via the reaction of alginic acid sodium salt with glycidyl methacrylate under acidic conditions, overnight at 60ºC, following a method proposed in literature[38]. These acidic conditions and the prolonged time of reaction are essential for the irreversible epoxide ring-opening of glycidyl methacrylate through the carboxylic acid groups[38,46].

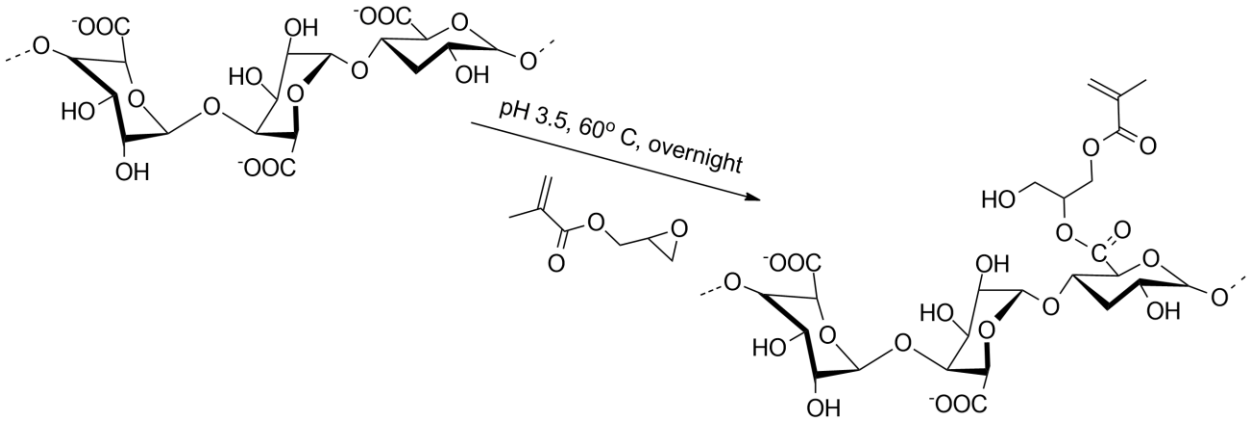

Scheme 3.4 – Alginate methacrylate synthesis reaction

The successful modification of the product was confirmed by the appearance of two new vinyl peaks in the ^{1}H-NMR spectrum in Figure 3.6.

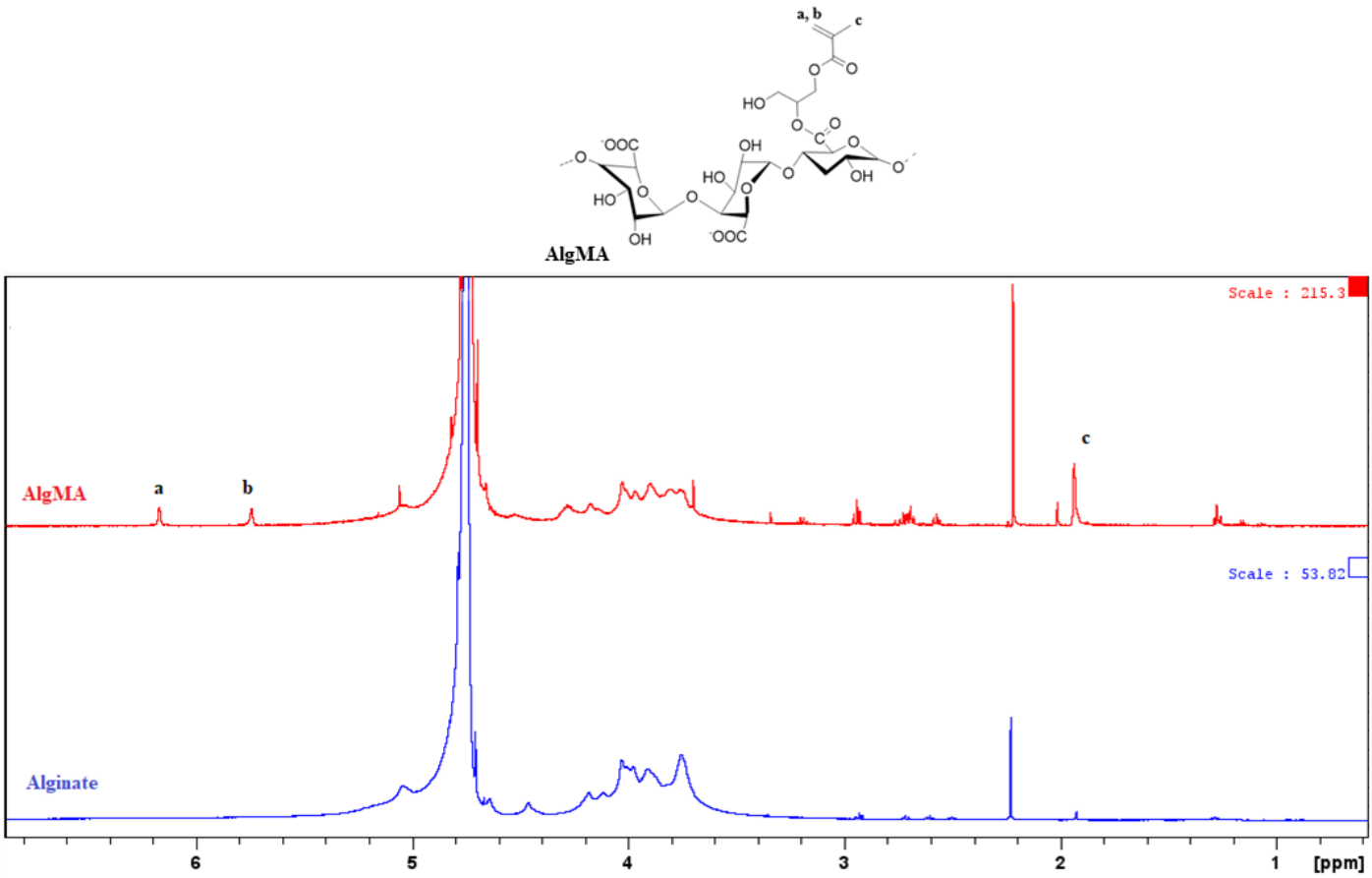

Figure 3.6 - ^{1}H-NMR spectra of Alginate methacrylate and Alginate in D_2O.

The resonances from guluronic and mannuronic units can be observed overlapping for both spectra. Two new peaks can be observed for AlgMA at 5.75 ppm and 6.17 ppm that correspond to the resonance of the vinyl protons of glycidyl methacrylate and the increased intensity of the 1.94 ppm peak (which appears to be split with a smaller peak at 2.04 ppm) can be attributed to the methyl protons of the group. The 5.75 ppm resonance integral was used to normalize the rest of the peak integrals and its value was set to 1, hence the 6.17 ppm integral was calculated by software to be 1.03 and the integral under the splits 1.94 and 2.04 peak was calculated equal to 2.91. Resonance placements and integral are in good agreement with the reported values in the bibliography[38,47].

3.4 Hydrogel Synthesis

Hydrogel synthesis was conducted via photopolymerization using the as-synthesized exfoliated g-C_3N_4 as a photoinitiator under UV irradiation.

First, hydrogels were synthesized by incorporating EGDMA as the crosslinker and next hydrogels were also synthesized in the absence of a crosslinker based on the self-crosslinking of the catechol groups of dopamine methacrylamide via hydrogen bonds or π-π stacking. Different molar ratios of the catechol baring monomer were used with respect to the moles of PEGMA and the different gelation times were documented and correlated with the presence of the two crosslinking mechanisms.

3.4.1 P(PEGMA-*co*-DMA) Hydrogels with EGDMA as a crosslinker

In the presence of EGDMA as a crosslinker, 5 gels with different molar ratios of DMA to PEGMA were synthesized.

The conditions employed for each gel and their approximate gelation times are summarized in Table 3.2

Table 3.2

Sample	PEGMA wt%	g-C_3N_4 wt%	DMA moles% to PEGMA	EGDMA wt% to total mass of monomers	Gelation Time (h)
gel0	33.3	0.03	0	5	10
gel2	33.3	0.03	2	5	10
gel5	33.3	0.03	5	5	4
gel10	33.3	0.03	10	5	3
gel20	33.3	0.03	20	5	2

It can be observed that as the molar content of DMA increases the gelation time decreases, and that can be attributed to the catechol crosslinking via hydrogen bonding or π-π stacking[48], that contributes to higher crosslinking degrees and thus shorter gelation times.

3.4.2 P(PEGMA-*co*-DMA) Hydrogels without crosslinker

In the absence of a specific crosslinker, two hydrogels with different molar ratios of DMA to PEGMA were also synthesized, namely 5% and 20%, using the same constant concentrations for PEGMA and g-C_3N_4 as they were mentioned in paragraph 3.3.1.

The conditions used for both gels are presented in Table 3.3 along with their approximate gelation times.

Table 3.3

Sample	PEGMA wt%	g-C_3N_4 wt%	DMA moles% to PEGMA	Gelation Time (h)
gel5wc	33.3	0.03	5	7.5
gel20wc	33.3	0.03	20	4

Similar observations as those in paragraph 3.3.1 can be made for the gelation time of the catechol crosslinked hydrogels, as an increase of the molar ratio of DMA to PEGMA and therefore a higher concentration of catechol groups resulted in a lower gelation time. Nevertheless, shorter gelation times were in overall observed for the hydrogels containing EGDMA compared to the respective samples without the additional crosslinker.

3.5 Hydrogel Swelling Studies

The swelling behavior of synthesized P(PEGMA-*co*-DMA) hydrogels with and without crosslinker was assessed in PBS. The respective graphs are shown in Figures 3.7 to 3.11.

In Figure 3.7 (a) the swelling behavior over time of the gels 5%, 10% and 20% molar ratio DMA to PEGMA synthesized via the incorporation of EGDMA can be observed. As expected, as the molar ratio of DMA to PEGMA increases, and hence the degree of crosslinking also increases, the maximum swelling degree decreases. Both gel5 and gel10 reach their swelling plateau at approximately 5 hours, while gel20 reaches swelling plateau at approximately 2 hours.

Similar observations can be made for the swelling behavior of the gels synthesized in the absence of a crosslinker (Figure 3.7 (b)), where the crosslinking mechanism relies on the catechol groups, though the difference in the maximum degree of swelling between the less crosslinked gel5wc and the more crosslinked gel20wc seems to be very small.

The comparisons of the swelling behavior of the gels that were synthesized using comparable molar ratios of DMA to PEGMA with and without EGDMA are presented in Figures 3.8 and 3.9 for 20% and 5% molar ratio respectively. For gel20 and gel20wc the respective maximum swelling degrees, 1100% and 2160%, reveal a significant difference and an almost two-fold increase for the gel synthesized without crosslinker. For gel5 and gel5wc, the swelling behavior appears more similar with corresponding maximum swelling degrees of 2000% and 2300%, exhibiting only a 300% difference.

All the results are in good agreement with the differences in the crosslinking density expected from the reaction conditions followed for the synthesis of the hydrogels with varying DMA contents and in the presence or absence of EGDMA. Figures 3.10 and 3.11 are presented here to illustrate the repeatability of the swelling studies.

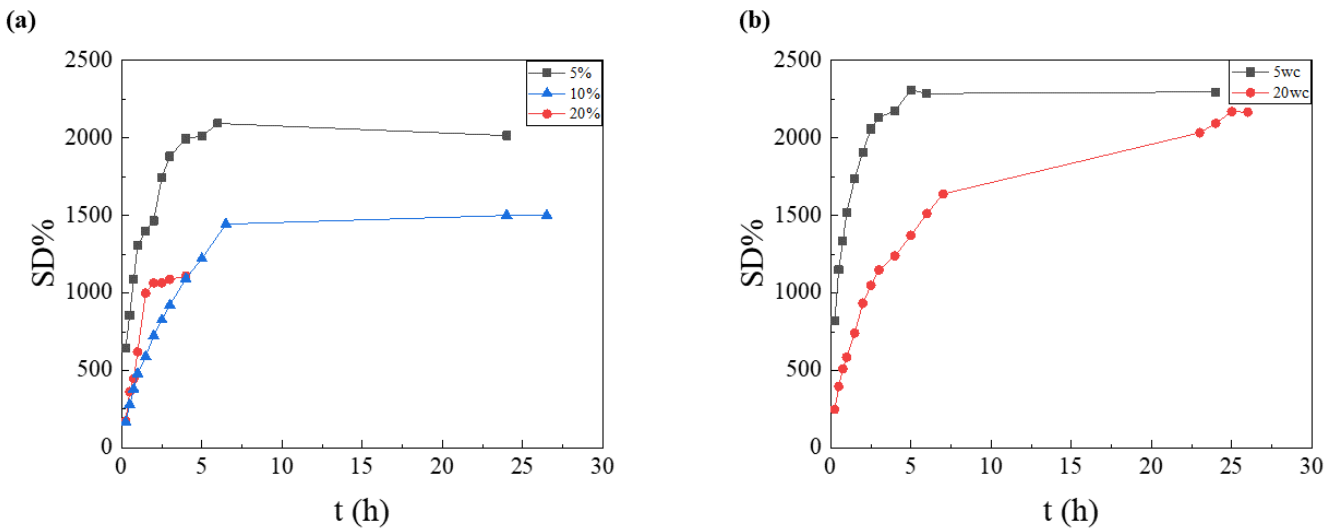

Figure 3.7 –(a) Swelling Degree over time of P(PEGMA-*co*-DMA) hydrogels, with a 5%, 10% and 20% molar ratio of DMA to PEGMA, in presence of EGDMA as crosslinker. (b) Swelling Degree over time of P(PEGMA-*co*-DMA) hydrogels, with a 5% (denoted as 5wc) and 20% (denoted 20wc) molar ratio of DMA to PEGMA, synthesized without crosslinker.

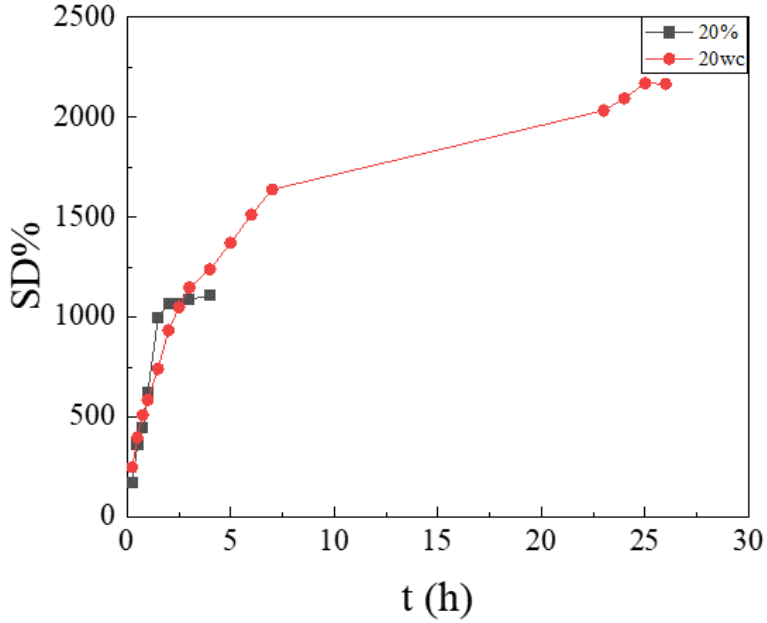

Figure 3.8 – Swelling Degree over time of P(PEGMA-*co*-DMA) hydrogels with a 20% molar ratio of DMA to PEGMA, synthesized with (denoted as 20%) and without (denoted as 20wc) crosslinker.

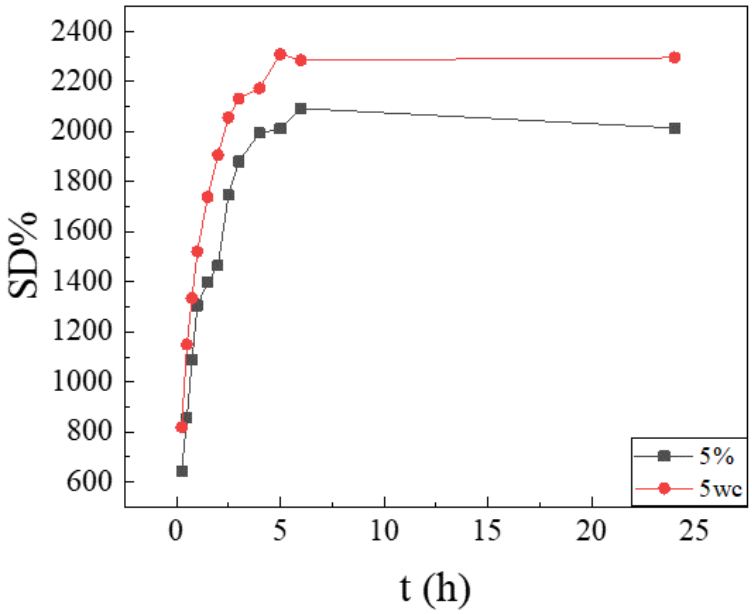

Figure 3.9 – Swelling Degree over time of P(PEGMA-*co*-DMA) hydrogels with a 5% molar ratio of DMA to PEGMA, synthesized with (denoted as 5%) and without (denoted as 5wc) crosslinker.

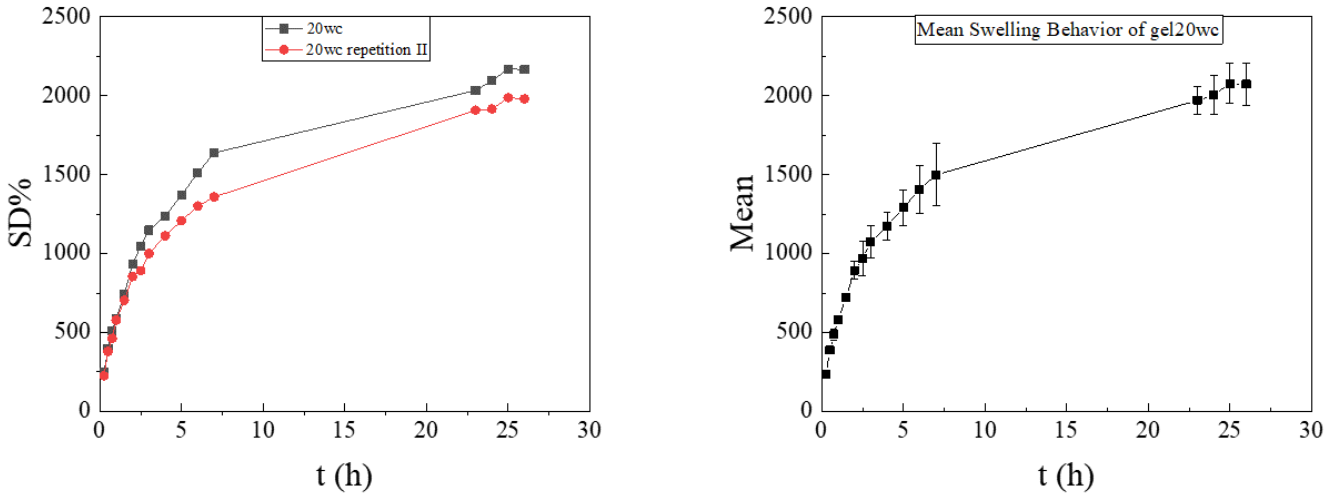

Figure 3.10 – Repeatability of swelling studies for P(PEGMA-*co*-DMA) gel20wc.

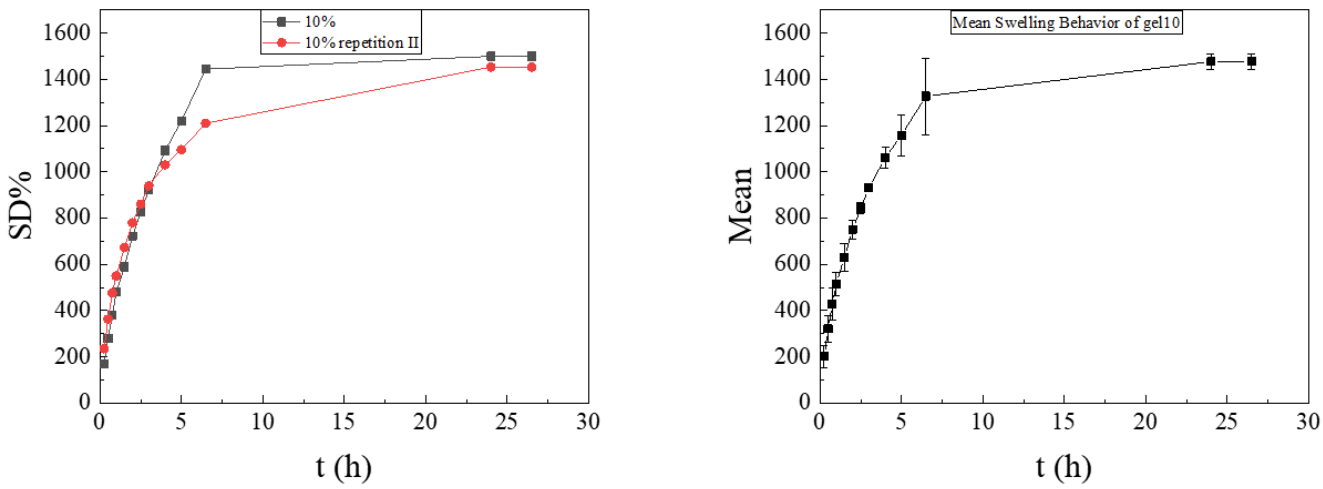

Figure 3.11 – Repeatability of swelling studies for P(PEGMA-*co*-DMA) gel10.

4.Conclusions and future studies

The aim of this first part of this thesis was to develop photopolymerizable hydrogels that can be photocured with visible light to be used in tissue engineering application. In this direction, the g-C_3N_4 visible light photoinitiator was synthesized via a green method without employing hard chemicals, to be used as a photoinitiator for the formation of hydrogels that will be used in tissue engineering studies. Different layered structures of the initiator were synthesized (bulk, thermally exfoliated and nanosheets), and their physicochemical properties were investigated, as well as their cytocompatibility (over 60% cell viability after 48h).

Also, dopamine methacrylamide, a photopolymerizable derivative of the well-known mussel inspired tissue adhesive dopamine was successfully synthesized, in order to be incorporated in the photopolymerizable hydrogels. Two more biocompatible photopolymerizable monomers were synthesized and characterized, gelatin methacrylamide with degrees of modification of 22.1% and 44.3% and alginate methacrylate, in order to be used as comonomers with dopamine methacrylamide.

Hydrogels of PEGMA (M_w=475) with DMA employing a variety of molar ratios of DMA to PEGMA, namely 0%, 2%, 5%, 10% and 20% were synthesized, via free-radical photopolymerization using the g-C_3N_4 as photoinitiator, in the presence of EGDMA as a crosslinker. Similarly, hydrogels of PEGMA(M_w=475) with DMA were with molar ratios of DMA to PEGMA 5% and 20% were photopolymerized with the same photoinitiator but in the absence of a crosslinker. In both synthetic procedures gelation was achieved, thus hydrogels can be obtained without employing any additional crosslinker by exploiting the self-crosslinking properties of the catechol moieties.

The swelling behavior of the gels with and without additional crosslinking was assessed, with the latter yielding higher maximum degrees of swelling, i.e., 2300 and 2100 for 5% and 20% respectively due to lower crosslinking degrees.

In the current studies, versatile crosslinking of these hydrogels is being investigated via the incorporation of iron-catechol complexes that will award the resulting hydrogels with self-healing properties. Next, the already synthesized hydrogels will be used in cell cultures to assess their biocompatibility and cell

proliferation capacities. For future experiments, the other two synthesized natural macromers will be further characterized and employed in the preparation of hydrogels for cell culture experiments.

Bibliography and Citations

1. Mozafari, M., Sefat, F. & Atala, A. Handbook of Tissue Engineering Scaffolds: Volume One. 759.
2. Mason, C. & Dunnill, P. A brief definition of regenerative medicine. *Regenerative Medicine* **3**, 1–5 (2008).
3. Khademhosseini, A. & Langer, R. A decade of progress in tissue engineering. *Nat Protoc* **11**, 1775–1781 (2016).
4. O'Brien, F. J. Biomaterials & scaffolds for tissue engineering. *Materials Today* **14**, 88–95 (2011).
5. *Biomedical Applications of Hydrogels Handbook*. (Springer New York, 2010). doi:10.1007/978-1-4419-5919-5.
6. Williams, D. F. On the mechanisms of biocompatibility. *Biomaterials* **29**, 2941–2953 (2008).
7. Jurak, M., Wiącek, A. E., Ładniak, A., Przykaza, K. & Szafran, K. What affects the biocompatibility of polymers? *Advances in Colloid and Interface Science* **294**, 102451 (2021).
8. Hutmacher, D. W. Sca!olds in tissue engineering bone and cartilage. 15 (2000).
9. Zhang, F. & King, M. W. Biodegradable Polymers as the Pivotal Player in the Design of Tissue Engineering Scaffolds. *Adv. Healthcare Mater.* **9**, 1901358 (2020).
10. Bauer, S., Schmuki, P., von der Mark, K. & Park, J. Engineering biocompatible implant surfaces. *Progress in Materials Science* **58**, 261–326 (2013).
11. Kanwar, S. & Vijayavenkataraman, S. Design of 3D printed scaffolds for bone tissue engineering: A review. *Bioprinting* **24**, e00167 (2021).
12. Reddy, M. S. B., Ponnamma, D., Choudhary, R. & Sadasivuni, K. K. A Comparative Review of Natural and Synthetic Biopolymer Composite Scaffolds. *Polymers* **13**, 1105 (2021).
13. Poorna, M. R., Jayakumar, R., Chen, J.-P. & Mony, U. Hydrogels: A potential platform for induced pluripotent stem cell culture and differentiation. *Colloids and Surfaces B: Biointerfaces* **207**, 111991 (2021).
14. WICHTERLE, O. & LÍM, D. Hydrophilic Gels for Biological Use. *Nature* **185**, 117–118 (1960).
15. Nguyen, K. T. & West, J. L. Photopolymerizable hydrogels for tissue engineering applications. *Biomaterials* **23**, 4307–4314 (2002).
16. Kaur, M. & Srivastava, A. K. PHOTOPOLYMERIZATION: A REVIEW. *Journal of Macromolecular Science, Part C: Polymer Reviews* **42**, 481–512 (2002).
17. Chiulan, I., Heggset, E. B., Voicu, Ş. I. & Chinga-Carrasco, G. Photopolymerization of Bio-Based Polymers in a Biomedical Engineering Perspective. *Biomacromolecules* **22**, 1795–1814 (2021).
18. Lago, M. A. *et al.* Photoinitiators: a food safety review. *Food Additives & Contaminants: Part A* 1–20 (2015) doi:10.1080/19440049.2015.1014866.
19. Mendes-Felipe, C., Oliveira, J., Etxebarria, I., Vilas-Vilela, J. L. & Lanceros-Mendez, S. State-of-the-Art and Future Challenges of UV Curable Polymer-Based Smart Materials for Printing Technologies. *Adv. Mater. Technol.* **4**, 1800618 (2019).
20. Wang, X. *et al.* A metal-free polymeric photocatalyst for hydrogen production from water under visible light. *Nature Mater* **8**, 76–80 (2009).
21. Hang, Z., Yu, H., Luo, L. & Huai, X. Nanoporous g-C3N4/MOF: high-performance photoinitiator for UV-curable coating. *J Mater Sci* **54**, 13959–13972 (2019).

22. Kiskan, B., Zhang, J., Wang, X., Antonietti, M. & Yagci, Y. Mesoporous Graphitic Carbon Nitride as a Heterogeneous Visible Light Photoinitiator for Radical Polymerization. *ACS Macro Lett.* **1**, 546–549 (2012).
23. Cao, Q., Kumru, B., Antonietti, M. & Schmidt, B. V. K. J. Graphitic carbon nitride and polymers: a mutual combination for advanced properties. *Mater. Horiz.* **7**, 762–786 (2020).
24. Hao, Q. *et al.* Graphitic carbon nitride with different dimensionalities for energy and environmental applications. *Nano Res.* **13**, 18–37 (2020).
25. Barrio, J., Volokh, M. & Shalom, M. Polymeric carbon nitrides and related metal-free materials for energy and environmental applications. *J. Mater. Chem. A* **8**, 11075–11116 (2020).
26. Kumru, B., Shalom, M., Antonietti, M. & Schmidt, B. V. K. J. Reinforced Hydrogels via Carbon Nitride Initiated Polymerization. *Macromolecules* **50**, 1862–1869 (2017).
27. Liu, J. *et al.* Carbon nitride nanosheets as visible light photocatalytic initiators and crosslinkers for hydrogels with thermoresponsive turbidity. *J. Mater. Chem. A* **5**, 8933–8938 (2017).
28. Sun, J., Schmidt, B. V. K. J., Wang, X. & Shalom, M. Self-Standing Carbon Nitride-Based Hydrogels with High Photocatalytic Activity. *ACS Appl. Mater. Interfaces* **9**, 2029–2034 (2017).
29. Zhang, X. *et al.* Enhanced Photoresponsive Ultrathin Graphitic-Phase C_3N_4 Nanosheets for Bioimaging. *J. Am. Chem. Soc.* **135**, 18–21 (2013).
30. Lin, L.-S. *et al.* Graphitic-phase C3N4 nanosheets as efficient photosensitizers and pH-responsive drug nanocarriers for cancer imaging and therapy. *J. Mater. Chem. B* **2**, 1031 (2014).
31. Svoboda, L. *et al.* Crucial cytotoxic and antimicrobial activity changes driven by amount of doped silver in biocompatible carbon nitride nanosheets. *Colloids and Surfaces B: Biointerfaces* **202**, 111680 (2021).
32. Yang, G. *et al.* Improved corrosion resistance and biocompatibility of biodegradable magnesium alloy by coating graphite carbon nitride (g-C3N4). *Journal of Alloys and Compounds* **770**, 823–830 (2019).
33. Tiwari, J. N. *et al.* Accelerated Bone Regeneration by Two-Photon Photoactivated Carbon Nitride Nanosheets. *ACS Nano* **11**, 742–751 (2017).
34. Yan, S. C., Li, Z. S. & Zou, Z. G. Photodegradation Performance of g-C_3N_4 Fabricated by Directly Heating Melamine. *Langmuir* **25**, 10397–10401 (2009).
35. Niu, P., Zhang, L., Liu, G. & Cheng, H.-M. Graphene-Like Carbon Nitride Nanosheets for Improved Photocatalytic Activities. *Adv. Funct. Mater.* **22**, 4763–4770 (2012).
36. Glass, P., Chung, H., Washburn, N. R. & Sitti, M. Enhanced Reversible Adhesion of Dopamine Methacrylamide-Coated Elastomer Microfibrillar Structures under Wet Conditions. *Langmuir* **25**, 6607–6612 (2009).
37. Van Den Bulcke, A. I. *et al.* Structural and Rheological Properties of Methacrylamide Modified Gelatin Hydrogels. *Biomacromolecules* **1**, 31–38 (2000).
38. Lima, D. S. *et al.* pH-responsive alginate-based hydrogels for protein delivery. *Journal of Molecular Liquids* **262**, 29–36 (2018).
39. Thomas, A. *et al.* Graphitic carbon nitride materials: variation of structure and morphology and their use as metal-free catalysts. *J. Mater. Chem.* **18**, 4893 (2008).
40. Li, Y. *et al.* Macroscopic Foam-Like Holey Ultrathin g-C_3N_4 Nanosheets for Drastic Improvement of Visible-Light Photocatalytic Activity. *Adv. Energy Mater.* **6**, 1601273 (2016).
41. Xu, J., Zhang, L., Shi, R. & Zhu, Y. Chemical exfoliation of graphitic carbon nitride for efficient heterogeneous photocatalysis. *J. Mater. Chem. A* **1**, 14766 (2013).

42. Kang, S. *et al.* An instant, biocompatible and biodegradable high-performance graphitic carbon nitride. *Journal of Colloid and Interface Science* **563**, 336–346 (2020).
43. Yue, K. *et al.* Structural analysis of photocrosslinkable methacryloyl-modified protein derivatives. *Biomaterials* **139**, 163–171 (2017).
44. Bernert, D. B., Isenbügel, K. & Ritter, H. Synthesis of a Novel Glycopeptide by Polymeranalogous Reaction of Gelatin with Mono-6- *para* -toluenesulfonyl-β-cyclodextrin and its Supramolecular Properties: Synthesis of a Novel Glycopeptide by Polymeranalogous Reaction …. *Macromol. Rapid Commun.* **32**, 397–403 (2011).
45. Ding, W. *et al.* The Influence of Shuttle-Shape Emodin Nanoparticles on the Streptococcus suis Biofilm. *Front. Pharmacol.* **9**, 227 (2018).
46. Hasany, M. *et al.* Synthesis, properties, and biomedical applications of alginate methacrylate (ALMA)-based hydrogels: Current advances and challenges. *Applied Materials Today* **24**, 101150 (2021).
47. Araiza-Verduzco, F. *et al.* Photocrosslinked Alginate-Methacrylate Hydrogels with Modulable Mechanical Properties: Effect of the Molecular Conformation and Electron Density of the Methacrylate Reactive Group. *Materials* **13**, 534 (2020).
48. Quan *et al.* Mussel-Inspired Catechol-Functionalized Hydrogels and Their Medical Applications. *Molecules* **24**, 2586 (2019).